Available online at www.sciencedirect.com
ScienceDirect
Composites Science and Technology 68 (2008) 1718–1726
COMPOSITES SCIENCE AND TECHNOLOGY
www.elsevier.com/locate/compscitech

Ablation behavior of ZrB_2–SiC ultra high temperature ceramics under simulated atmospheric re-entry conditions

Xinghong Zhang *, Ping Hu *, Jiecai Han, Songhe Meng

Center for Composite Materials, Harbin Institute of Technology, Harbin 150001, PR China

Received 4 June 2007; received in revised form 17 December 2007; accepted 6 February 2008
Available online 15 February 2008

Abstract

ZrB_2–20vol%SiC ultra high temperature ceramic (UHTC) was prepared by hot-pressing. Ablation tests of the flat-face models were conducted under ground simulated atmospheric re-entry conditions using arc-jet testing with heat fluxes of 1.7 MW/m^2 and 5.4 MW/m^2 under subsonic conditions, respectively. There was little weight or configuration change after ablation at a heat flux of 1.7 MW/m^2. However, ZrB_2–SiC composite underwent severe ablation and whose surface temperatures exceeded 2300 °C at a heat flux of 5.4 MW/m^2. Sharp-shape leading edge models were ablated under supersonic conditions with the stagnation pressure and Mach number of 1.2 atm and 2.7 M, respectively, and sharp-shaped leading edge C/SiC models were also ablated under the same condition for comparison. ZrB_2–SiC composite exhibited an excellent thermal-oxidative and configurational stability in the simulated re-entry environment compared with C/SiC material. Results indicate that ZrB_2–SiC ultra high temperature ceramics are the potential candidates for leading edges. The temperature limit for UHTC is controlled by the softening and degradation of the formed oxide scale.

Keywords: A. ZrB_2; A. SiC; B. Ablation behavior

1. Introduction

Ultra high temperature ceramics (UHTC) include some refractory metal diborides that were historically studied and developed since the 1960s and early 1970s [1–3]. Interest in UHTC has increased significantly in recent years because of the drive to produce thermal protection systems (TPS) and other components for hypersonic aerospace vehicles [4–8].

In contrast to traditional blunt capsules or Shuttle-type vehicles, characterized by poor gliding capabilities, the future use of UHTC opens new prospects for the development of space planes with slender fuselage noses and sharp wing leading edges. Vehicles with sharp leading edges and/or sharp noses have lower drag and higher lift to drag ratios (L/D) than blunt-nosed vehicles, but they also have to endure higher surface temperatures [9–12]. The lower drag should improve ascent performance, while the higher lift to drag produces a greater range for abort and re-entry trajectories. Improved range provides operational safety benefits for the system. Sharp leading edges have not been used for reusable vehicles in the past because materials able to repeatedly withstand the higher entry and abort temperatures were not available. Recent developments in the use of UHTC have given renewed hope to the eventual realization of sharp leading edge vehicles [13–15].

However, report on the ablation behavior of ZrB_2–SiC under simulated atmospheric re-entry conditions is limited and their surface temperatures are always less than 2000 °C. In this study, ZrB_2–20vol%SiC ultra high temperature ceramic was prepared by hot-pressing. The flat-face models together with sharp-shaped leading edge models were tested using an arc-jet facility under different conditions, and sharp-shaped leading edge C/SiC models were also ablated under the same condition for comparison. The purpose of this study is to investigate the ablation

* Corresponding authors. Tel./fax: +86 45186402382.
E-mail addresses: zhangxh@hit.edu.cn (X.H. Zhang), huping@hit.edu.cn (P. Hu).

0266-3538/$ - see front matter © 2008 Elsevier Ltd. All rights reserved.
doi:10.1016/j.compscitech.2008.02.009

behavior of the ZrB_2–SiC composite and the ablation mechanism is also discussed.

2. Experimental procedure

The samples used here for oxidation testing were fabricated from commercial ZrB_2 (Northwest Institute for Non-ferrous Metal Research, China) and SiC (Weifang Kaihua Micro-powder Co., Ltd., China) powders. The ZrB_2 and SiC powders had the same purity of 99.5%, with mean particle size of 5 μm and 2 μm, respectively. The powder mixture of ZrB_2 + 20vol% SiC was ball-milled in ethanol for 8 h using hard milling media and dried in a rotating evaporator. Milled powder was then uniaxially hot pressed in a boron nitride coated graphite die at 2000 °C for 60 min under vacuum and 30 MPa of applied pressure. The heating schedule has been described in detail elsewhere [16]. Bulk density and theoretical density were evaluated using the Archimedes method and the rule-of-mixture, respectively.

ZrB_2–SiC models with a cylindrical shape were cut from the billet, and then exposed to sustained enthalpy flows using an arc-jet facility with an average total enthalpy in the order of 10–30 MJ/kg. The facility is equipped with a 60 KW plasma torch which has a diameter of 30 mm of the exit nozzle that can be operated in air with a stagnation pressure of 0.03–0.5 atm. The dimension of the model is $\Phi 20 \times 30$ for the high heat flux under subsonic conditions and that of $\Phi 30 \times 30$ for the low heat flux. The ablation time for these models is 600 s. The heat fluxes were measured using flat-faced Gardon-type calorie meter and the measured fluxes for two flat-face models were 1.7 and 5.4 MW/m^2, respectively. The sharp leading edge models (Fig. 1) were also cut from the billet and then tested under supersonic conditions using an arc-heated wind tunnel that is operated in air. The size of the exit nozzle of the wind tunnel is 64 mm × 32 mm and the temperature of the supersonic flow was controlled in the temperature range of 1440–1450 °C. The stagnation pressure and Mach number of the supersonic flow at the exit nozzle were 1.2 atm and 2.7 M, respectively. The average total enthalpy is in the order of 2–4 MJ/kg.

The experiments were carried out with a two-colour Raytek pyrometer (RAYMR1SCSF, USA) which covers a temperature range of 1000–3000 °C. X-ray diffraction (Rigaku, Dmax-rb) and scanning electron microscopy/energy dispersive spectroscopy (FEI Sirion, Holand) were used to characterize the phase composition and the microstructure of the surface and the cross-section of the samples after testing.

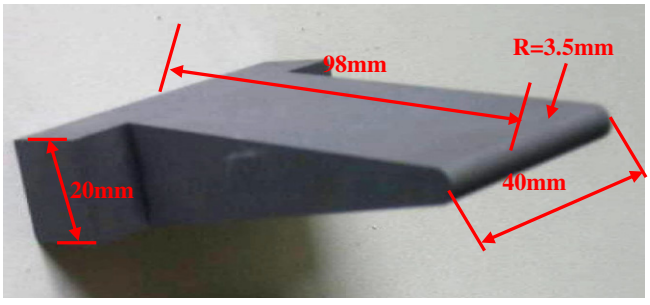

Fig. 1. Sharp-shape ZrB_2–SiC model used for arc-jet testing, curvature radius $R = 3.5$ mm.

3. Results and discussion

3.1. Microstructure of the hot-pressed composite

The bulk density of the sintered ZrB_2–SiC billets was 5.41 g/cm^3, which corresponds to a relative density higher than 98%. Fig. 2 shows a scanning electron micrograph of the polished surface of the ZrB_2–SiC composite. The microstructure of the composite is regular, in which the mean grain size is about 6 μm and the residual porosity is very scarce as shown in Fig. 2. The grain size of this material was estimated from the fracture surface of the composite (not shown). The SiC particulates, which represent the majority of the dark features in Fig. 2, are homogeneously dispersed in the ZrB_2 matrix and no agglomeration was detected. Exaggerated grain growth of ZrB_2 was restricted due to the existence of SiC particles. In addition, the introduction of SiC substantially enhanced densification of ZrB_2 during hot-pressing. ZrO_2 and B_2O_3 were assumed as the main oxygen carriers upon the surfaces of ZrB_2. Such a contamination by oxygen promotes vapor phase transport at temperatures below which mass transfer mechanisms like boundary/volume diffusion, which are much more effective than vapor phase for densification, start taking place; the anticipated coarsening decreases the driving force for densification at higher temperatures [17]. Densification of SiC-containing ZrB_2 powder mixtures initiates at lower temperatures compared with pure ZrB_2 as reactions with SiC are deemed to remove the oxide coatings, separating ZrB_2 particles from mutual contact.

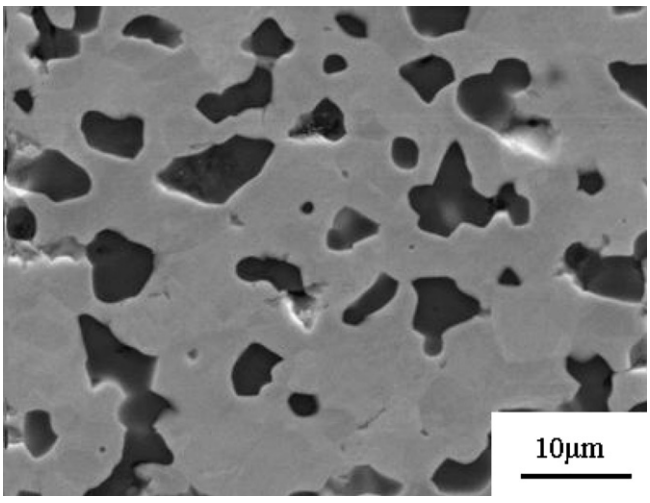

Fig. 2. SEM of the polished surfaces of the ZrB_2–SiC ultra high temperature ceramics.

Table 1
Summary of arc-jet sample characteristics, conditions and measured surface temperatures

Model (#)	Dimension (mm)	Heat flux (MW/m^2)	Weight change (%)	ΔThickness (mm)	Oxide scale (μm)	Ablation time (s)	Surface temperature (°C)
1	Φ30 × 30	1.7	0.00	0.00	25	600	1640–1660
2	Φ20 × 30	5.4	15.75	2.98	390	600	2150–2330

3.2. Microstructure changes and ablation properties of the composite

Characteristics of the two flat-face models after arc-jet testing are shown in Table 1. At a heat flux of 1.7 MW/m^2, no measurable weight change was observed, and steady state surface temperature was ~1650 °C as shown in Fig. 3. However, at a heat flux of 5.4 MW/m^2, there was severe oxidation and ablation after arc-jet testing and the maximum surface temperatures exceeded 2300 °C. A total weight loss of 15.75% was measured and the corresponding change in thickness was about 3 mm.

Fig. 4 shows the ZrB_2–SiC flat-face model before (a), during (b) and after (c) the ablation test under the heat flux of 1.7 MW/m^2. There was little change in the visual appearance of the surface and no appreciable structural change was detected. The surface micrograph shows the formation of bubbles (Fig. 5), which can be closely related to the release of gaseous oxidation by-products (i.e. CO and B_2O_3). The formation of bubbles may imply that the diffusion of the formed gaseous phases through the oxide layer is slower than that of O_2. In fact, during the initial exposure to such harsh convectively heating conditions, SiO, B_2O_3 and other highly volatile boron sub-oxides, which tend to evolve outside, most likely coalesced in bubbles inside the external forming glass [6]. Shear forces associated to the hot stream facilitated the bursting of bubbles and, for prolonged exposure, the smoothing of the outermost glassy coating. However, the surface was covered by a continuous glassy layer. The formation of an external silica based glassy layer is very effective in limiting the inward diffusion of oxygen into the inner bulk, thus enhancing the

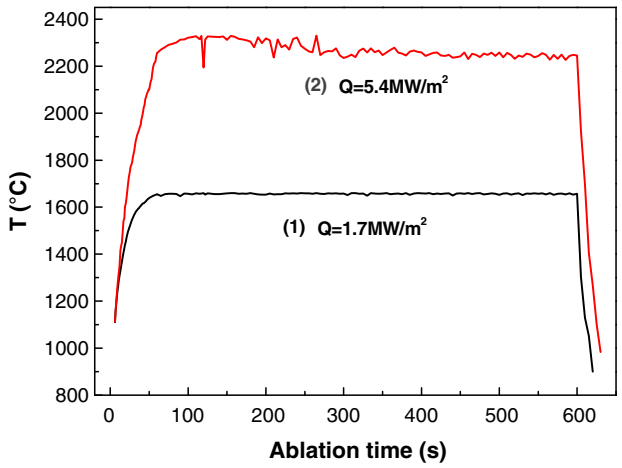

Fig. 3. Temperature curves vs. time during arc-jet testing of the flat-face ZrB_2–SiC models under the different heat fluxes.

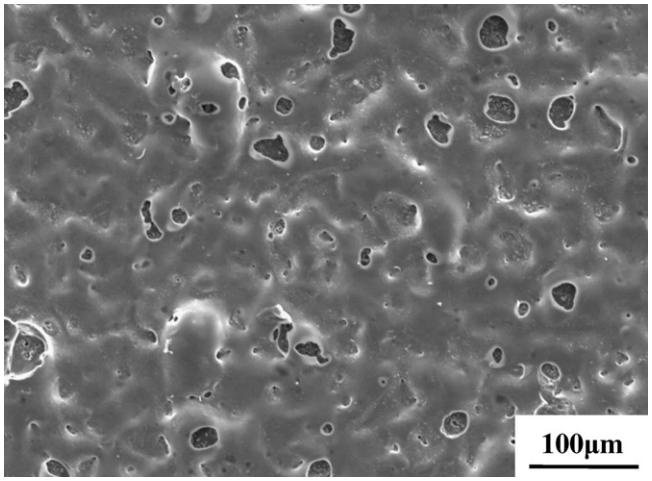

Fig. 5. SEM micrograph of the ablated flat-face ZrB_2–SiC model under a heat flux of 1.7 MW/m^2.

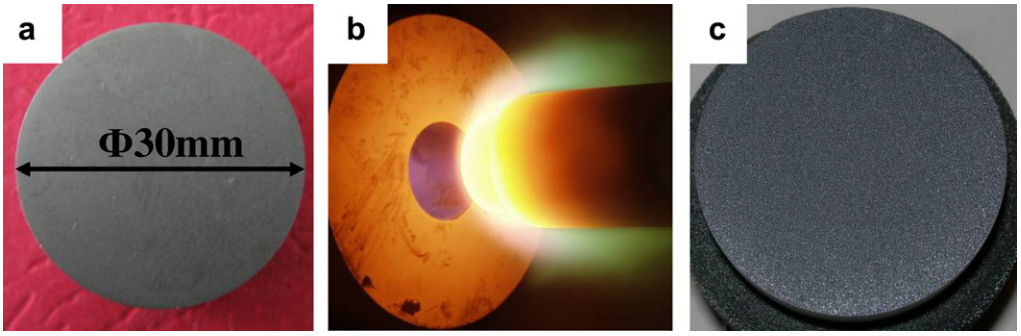

Fig. 4. Flat-face ZrB_2–SiC model before (a), during (b) and after (c) ablation test under a heat flux of 1.7 MW/m^2.

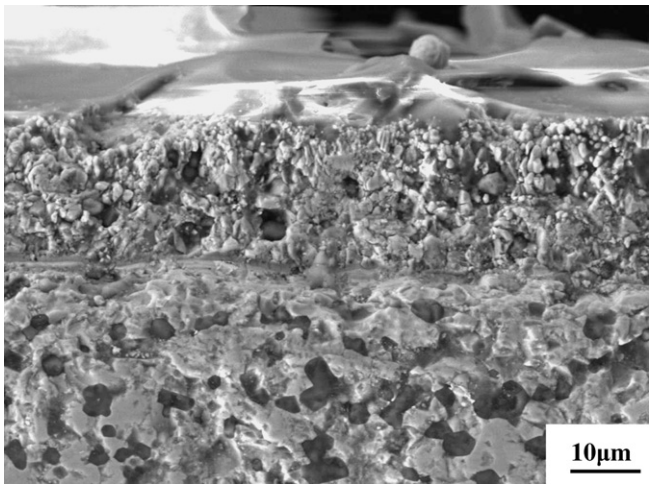

Fig. 6. Cross-sectional micrographs of the ablated flat-face ZrB_2–SiC model under a heat flux of 1.7 MW/m^2.

resistance to oxidation. The cross-section of the ZrB_2–SiC models after arc-jet testing at a heat flux of 1.7 MW/m^2 is shown in Fig. 6. Beneath the external glass layer, there was a subsurface layer about 25 μm thick containing zirconia. No SiC depletion layer was detected in the present case. In fact, during the exposure to such harsh heating, the models were subjected to mechanical loading besides oxidation. Silica alone cannot develop into a continuous glassy layer, and will be scoured away by gas flow due to the existence of the large shear forces during ablation process. The ZrO_2 appears to form a porous skeleton that does not enhance the oxidation protection, but it may provide mechanical integrity and strength to the liquid glass (i.e. silicate). Moreover, the ZrO_2 skeleton can provide a framework for the glass to be retained against the strong gas flow. The ablation rate is originally controlled by the chemical reaction of the surface ZrB_2 and SiC, and then by the oxygen diffusion through the glass layer and some porous regions and the evaporation of the glass. Therefore, most of the silica glass was retained during the ablation process and it was distributed in the zirconia grain boundary and the surface, which provides increased inhibition of the inward access of oxygen.

The macrographs of the specimen during and after the ablation test for 600 s at the heat flux of 5.4 MW/m^2 are shown in Fig. 7. A large amount of the molten oxidation product was blown away during the ablation process, resulting in a high erosion rate and marked change in the configuration (Fig. 7). The surface of the ablated sample was not smooth and exhibited a mechanical scour as a result of the airflow. Shear forces associated with the hot stream facilitated the erosion of the outermost glass coating. It should be noted that the edge of the ablated surface exhibited a higher erosion rate compared with the central region. This phenomenon can be explained by the higher heat flux and shear force at the edge compared with those at the center. Moreover, the high heat flux will result in a high temperature at the surface of the sample. Apparently, the high temperature decreases the viscosity of glass and accelerates the chemical reaction, leading to the increased oxidation and ablation rates. Fig. 8 is a micrograph of the ablated surface, which shows the formation of large holes with a diameter of ~30 μm. The surface was covered by a limited amount of discontinuous silica glass. Under this ablation condition, the SiO_2 layer formed on the

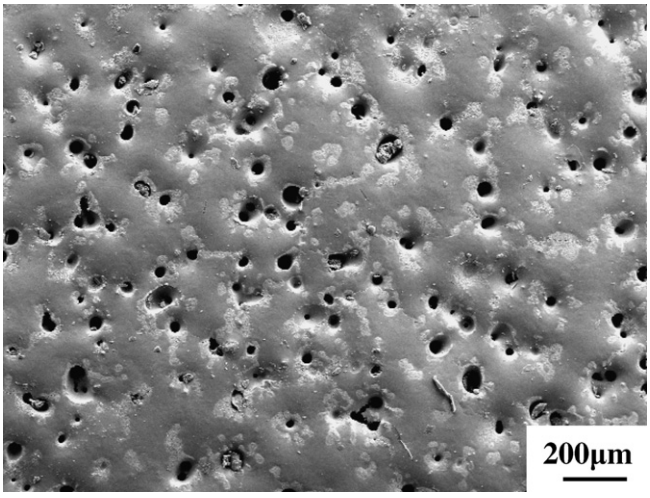

Fig. 8. SEM micrograph of the ablated flat-face ZrB_2–SiC model under a heat flux of 5.4 MW/m^2.

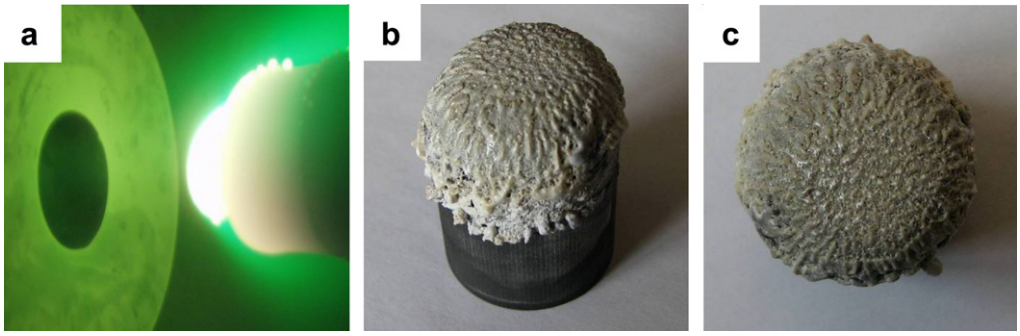

Fig. 7. Flat-face ZrB_2–SiC model during (a) and after (b and c) ablation test under a heat flux of 5.4 MW/m^2.

surface shows a very low viscosity and a significant evaporation rate due to the extreme high ablation temperature (>2300 °C), which leads to the intense degradation of the protective effect.

The cross-section of the models after arc-jet testing at the heat flux of 5.4 MW/m^2 provided insight into microstructure details of great interest (Fig. 9). Three distinct layers were detected, which is different from reported layered structure in previous studies [18–20]. The outermost layer (350 μm thick) was rather compact except for a few large pores. However, this layer was not adhered to an oxide sub-scale. Compositional analysis by EDS showed that the oxide was mainly composed of Zr, O and a little Si. ZrO_2 coalesced together by recrystallization under the present condition. Some silica glass was embedded within the compact ZrO_2. The formation of this layer effectively inhibited inward transport of oxygen. Passive oxidation protection is provided by the continuous compact ZrO_2 layer that effectively prevents direct exposure of the ZrB_2–SiC composite to air in this temperature region. Underlying this layer was a porous layer, which is a transitional region between the SiC-depleted layer and external oxide layer. The creation of such an inner porous layer was most likely caused by the oxidation of ZrB_2 since the formed ZrO_2 cannot adhere to the virgin matrix at high temperature. Obviously, cracking and spalling tend to occur in this region due to the weak bonding and CTEs mismatch between the oxide scale and unaltered ZrB_2 matrix. Underneath, a layer partly depleted of SiC (25 μm thick) was formed. The formation of SiC depletion

Table 2
Summary of arc-jet sample characteristics, conditions and measured surface temperatures

Model (#)	Pressure (MPa)	Mach number (M)	Weight change (%)	Ablation time (s)	Surface temperature (°C)
3	1.26	2.7	0.03	200	1445–1451
4	1.26	2.7	8.3	100	1443–1450

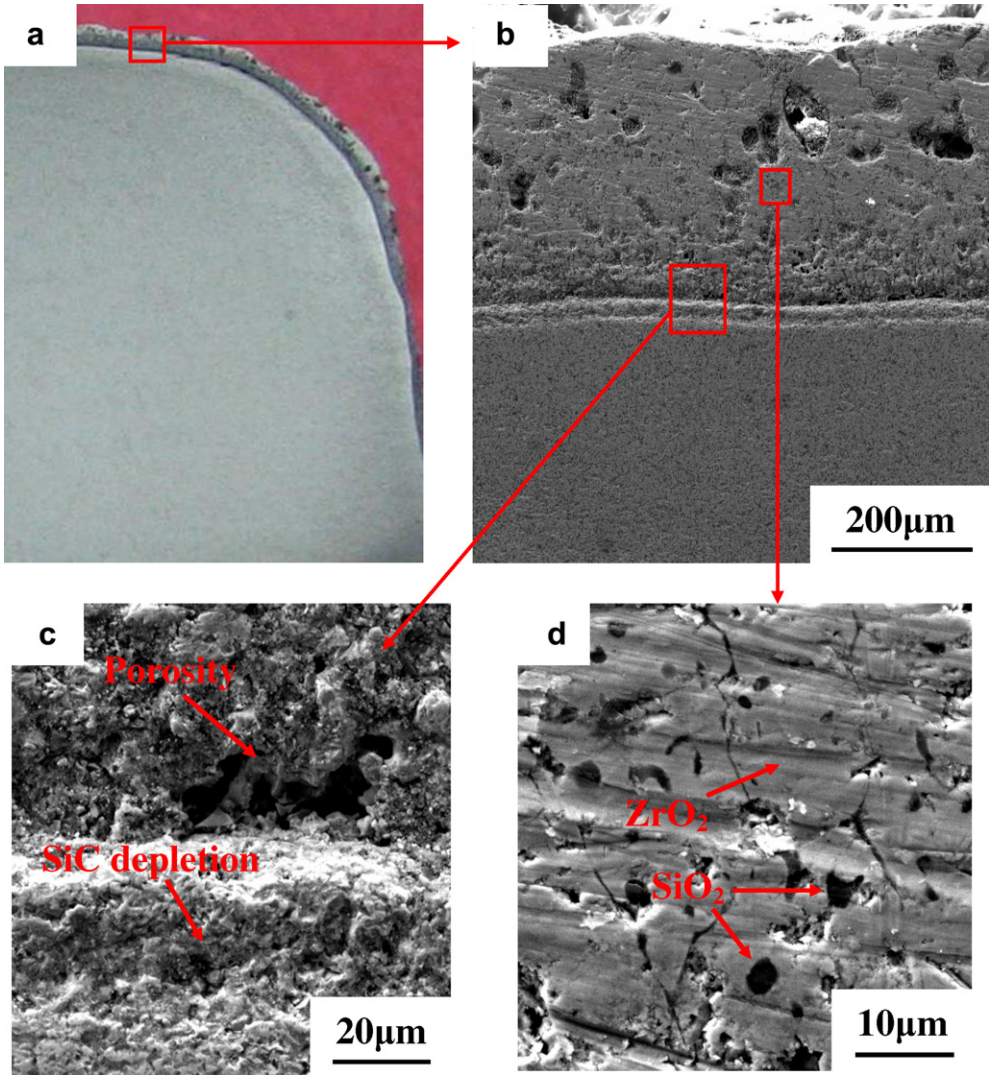

Fig. 9. Cross-sectional morphologies of the ablated flat-face ZrB_2–SiC model under a heat flux of 5.4 MW/m^2.

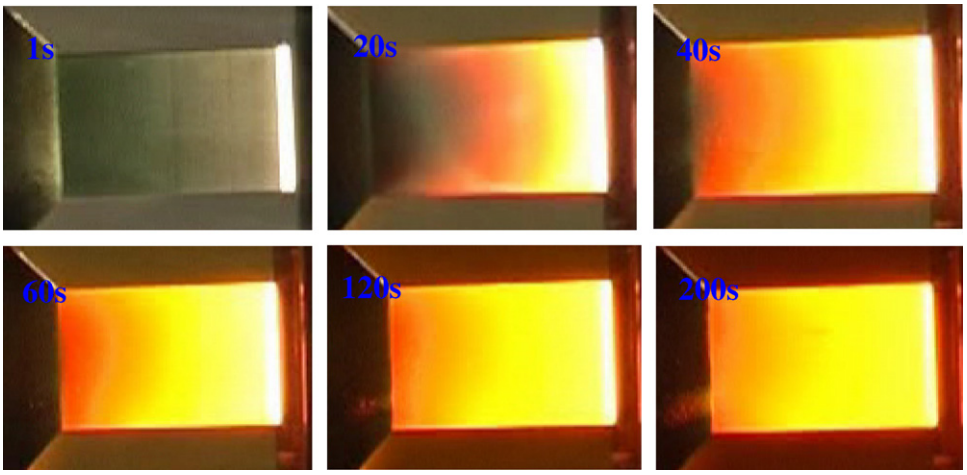

Fig. 10. Photographs of the ZrB_2–SiC sharp leading edge model at different testing times.

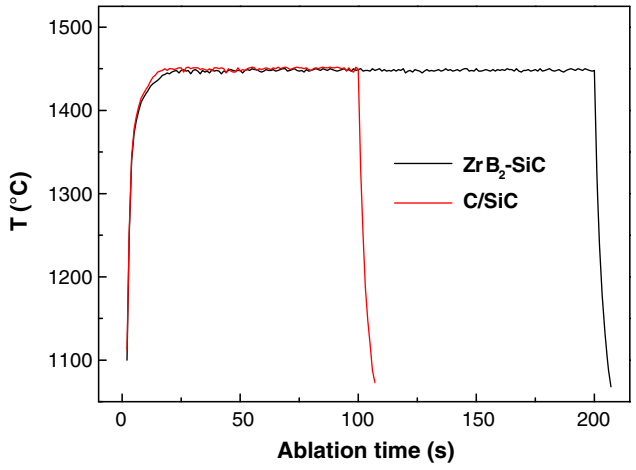

Fig. 11. Temperature curves vs. time during arc-jet testing of the sharp leading edge models.

layer was caused by the active oxidation of SiC, which represents a well-known phenomenon in SiC and SiC-containing zirconium diboride-based materials [13,18–20].

The ablation conditions for sharp leading edge models at the supersonic flow arc-heated wind tunnel are listed in Table 2. Fig. 10 shows the macrographs of the ZrB_2–SiC (model 3) sharp leading edge model at different testing times. The surface temperature increased drastically in a very short time when the samples were exposed to the arc-heated wind tunnel (Fig. 11). Specifically, the surface temperature rose dramatically to 1350 °C, in mere 3 s, and then rose gradually, until reached a steady temperature of ~1450 °C. As a result of the large temperature gradient, a high thermal stress occured. However, no cracks were observed on the sample. This fact suggests that the composite exhibits excellent thermal shock resistance. There was a marked change in the color distribution of the model in the initial 40 s, which then reached a steady state at 60 s, indicating that the temperature distribution on the surface of the model achieved a steady state after 60 s of heating. A similar trend was observed in the C/SiC composite (model 4) (Fig. 12). But the time to reach steady state of 40 s was less than that for model 3. The shorter time to reach steady state is probably due to its low thermal conductivity com-

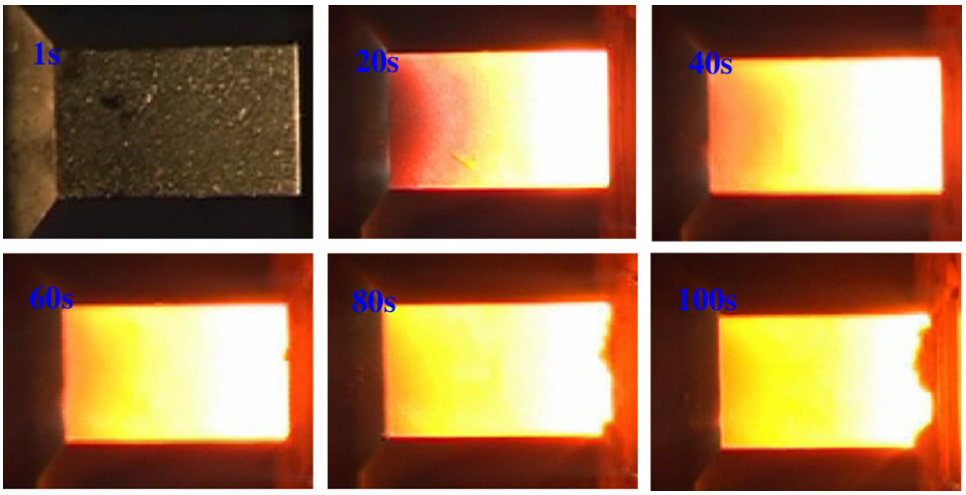

Fig. 12. Photographs of the C/SiC sharp leading edge model at different testing times.

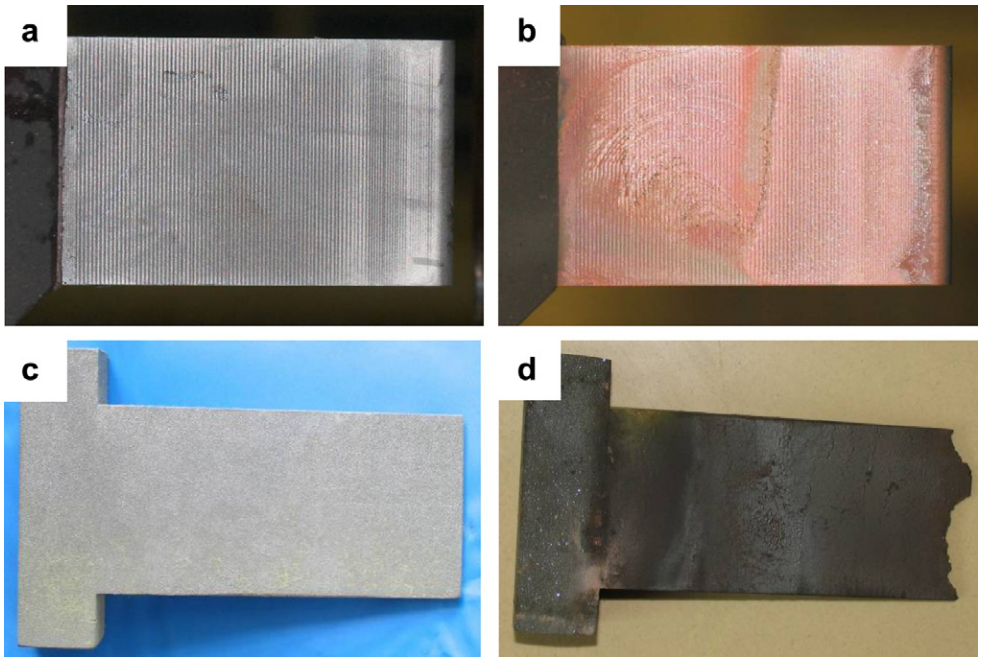

Fig. 13. Photographs of the sharp leading edge models before ((a) and (c)) and after ((b) and (d)) ablation testing. (a) and (b): ZrB_2–SiC, (c) and (d): C/SiC.

pared with ZrB_2–SiC. No configurational change during and after arc-jet testing was detected for model 3 as shown in Figs. 10 and 13b. This is quite beneficial to practical flight performances. For model 4, C/SiC composite began to severely ablate at 60 s and structural shape was remarkably destroyed as the ablation proceeded. The weight change was up to 8.3% after arc-jet testing while it was only 0.03% for model 3. Moreover, the structural shape was significant ablated as shown in Fig. 13d. High oxidation resistance coupled with configurational stability of the present UHTC when subjected to supersonic flow and heat fluxes typical of a re-entry environment make it a good candidate for use in aerospace applications, especially for sharp-shaped structures like wing leading edges and nose caps.

3.3. Ablation mechanism

During atmospheric re-entry, space vehicle will undergo severe aerothermodynamic heating resulting in high temperature on the outer surfaces of the materials. There were severe reactions between the reactive gases and the ZrB_2–SiC composite. In the present case, the main expected reactions during the oxidation process are as follows:

$$ZrB_2(s) + \frac{5}{2}O_2(g) \rightarrow ZrO_2(s) + B_2O_3(l) \quad (1)$$

$$B_2O_3(l) \rightarrow B_2O_3(g) \quad (2)$$

$$SiC(s) + \frac{3}{2}O_2(g) \rightarrow SiO_2(l) + CO(g) \quad (3)$$

$$SiC(s) + O_2(g) \rightarrow SiO(g) + CO(g) \quad (4)$$

$$SiC(s) + 2SiO_2(l) \rightarrow 3SiO(g) + CO(g) \quad (5)$$

$$SiO_2(l) \rightarrow SiO_2(g) \quad (6)$$

In fact, B_2O_3 has an unusually low melting point (450 °C) and a high vapor pressure (Fig. 14). Therefore, at high temperature, B_2O_3 vaporizes quickly. The rapid volatilization of B_2O_3 results in increased oxidation of ZrB_2 since ZrO_2 is not a highly protective oxide. The introduction of SiC remarkably improves the oxidation resistance of the ZrB_2 material above 1200 °C due to the formation of silica glass (Reaction (3) which is more viscous, having a higher melting temperature and a lower vapor pressure, and more resistant to oxygen diffusion [18–20]. The significant improvement in oxidation resistance of ZrB_2 based UHTC below 2000 °C has been achieved by the incorporation of SiC due to the formation of a silica glass layer with low oxygen permeability, which provides an efficacious protective oxidation barrier. Apart

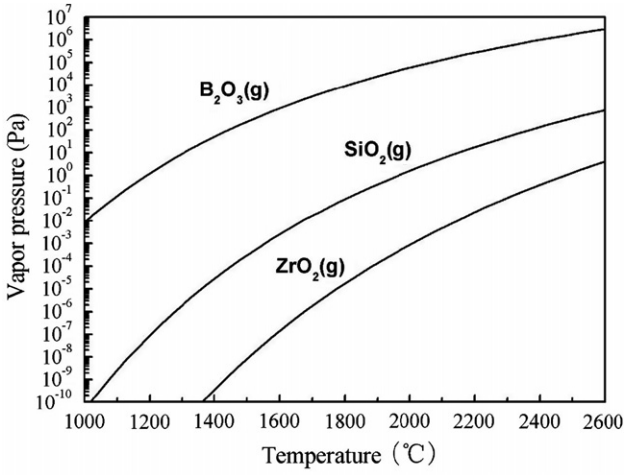

Fig. 14. Vapor pressure vs. temperature for the above oxides, calculated at ambient pressure.

from aerothermal loads, the materials are also subjected to large aerodynamic loads during hypersonic flight. Therefore, the mechanical loads should be taken into account, as well as oxidation, during practical operations. ZrO_2 provides an oxide framework without blown away by the gas flow leading to the configurational stability of the material. The combination of ZrO_2 and SiO_2 is responsible for configurational stability coupled with high oxidation resistance of the present UHTC when subjected to simulated atmospheric re-entry conditions. However, the efficiency of SiC significantly decreased at higher temperatures, especially above 2200 °C, because of the active oxidation (Reactions (4) and (5) and rapid evaporation (Reaction (6)) due to high vapor pressure (Fig. 14). Moreover, the existence of the large amount of silica will significantly lower the melting point of ZrO_2–SiO_2, which causes a strength loss of the formed oxide scale resulting in spallation or peeling under aerodynamic loads.

Apparently, the present UHTC cannot maintain the passivating protective capability at extremely high temperatures (i.e. >2300 °C) since the formed oxide scale is not stable under the aerothermodynamic loads. The temperature limit for SiC reinforced ZrB_2 based UHTC is mostly dependent on the softening and degradation of ZrO_2 based oxide scale, which is also controlled by SiC content since the melting point of the ZrO_2 based oxide scale is closely connected with SiO_2 content. When the shear forces exceed the strength of the formed oxide framework, the oxides peel off or dislodge from the specimens resulting in increased oxidation and degradation of configuration, which in turn affect the performance and safety of the vehicles. The softening and degradation of oxide scale resulted from increased temperatures is a major issue of the UHTC for use in extreme environments like those associated with hypersonic flight, atmospheric re-entry and rocket propulsion. In this respect, the content of the low melting point oxides can be reduced to improve the upper limit of the service temperatures. High SiC content is beneficial for the performance of the UHTC at low temperatures, whereas low SiC content is favorable for the use of the UHTC at high temperatures. Therefore, the compositions of reinforced phases (i.e. SiC) should be optimized according to the practical service environment, with damage within acceptable limits.

The coherence between oxide scale and unaltered material is another critical issue. As can be seen from Fig. 9, many defects like pores existed in the inner material which may lead to the rupture of the whole oxide scale. The extent of the damage under these conditions is to be considered unacceptable for the foreseen demands of reliability and re-usability at extremely high temperatures (i.e. above 2300 °C).

4. Conclusions

An ultra high temperature dense ZrB_2–SiC ceramic was produced by hot-pressing. ZrB_2–SiC models were exposed to ground simulated atmospheric re-entry conditions using arc-jet testing with heat fluxes of 1.7 MW/m^2 and 5.4 MW/m^2, respectively. For temperatures in the order of 1600–1700 °C, the material was able to endure the heating conditions, thanks to the formation of an external multiphase oxide scale. However, for temperatures in the order of 2300 °C, evident oxidation and ablation occured and the material was unable to offer a valuable resistance to the applied aerothermal load. ZrB_2–SiC ultra high temperature ceramics also exhibited an excellent thermal-oxidative and configurational stability under supersonic conditions compared with the C/SiC material, which suggests they are potential candidates for leading edges. Results indicate that ZrB_2–SiC can maintain the high oxidation resistance coupled with configurational stability at temperatures lower than that point which results in significant softening and degradation of the oxide scale, and that point will be the temperature limit for UHTC.

Acknowledgements

This work was supported by the National Natural Science Foundation of China (90505015 and 50602010), the Research Fund for the Doctoral Program of Higher Education (20060213031) and the Program for New Century Excellent Talents in University.

References

[1] Kuriakose AK, Margrave JL. The oxidation kinetics of zirconium diboride and zirconium carbide at high temperatures. J Electrochem Soc 1964;111(7):827–31.
[2] Tripp WC, Davis HH, Graham HC. Effect of a SiC addition on the oxidation of ZrB_2. Am Ceram Soc Bull 1973;52(8):612–6.
[3] Hinze JW, Tripp WC, Graham HC. High-temperature oxidation behavior of a HfB_2 plus 20 v/o SiC composite. J Electrochem Soc 1975;122(9):1249–54.
[4] Chamberlain AL, Fahrenholtz WG, Hilmas GE, Ellerby DT. Characterization of zirconium diboride for thermal protection systems. Key Eng Mater 2004;264–268(I):493–6.
[5] Opeka MM, Talmy IG, Zaykoski JA. Oxidation-based materials selection for 2000 °C + hypersonic aerosurfaces: theoretical considerations and historical experience. J Mater Sci 2004;39(19):5887–904.
[6] Monteverde F, Savino R. Stability of ultra-high-temperature ZrB_2 – SiC ceramics under simulated atmospheric re-entry conditions. J Euro Ceram Soc 2007;27(16):4797–805.
[7] Van Wie DM, Drewry Jr DG, King DE, Hudson CM. The hypersonic environment: required operating conditions and design challenges. J Mater Sci 2004;39(19):5915–24.
[8] Monteverde F. The thermal stability in air of hot-pressed diboride matrix composites for uses at ultra-high temperatures. Corros Sci 2005;47(8):2020–33.
[9] Savino Raffaele, De Stefano Fumo Mario, Paterna Diego, Serpico Michelangelo. Aerothermodynamic study of UHTC-based thermal protection systems. Aero Sci Tech 2005;9:151–60.
[10] Monti Rodolfo, De Stefano Fumo Mario, Savino Raffaele. Thermal shielding of a re-entry vehicle by UHTC materials. In: AIAA/CIRA 13th international space planes and hypersonics systems and Technolo, AIAA; 2005. p. 3265.
[11] Lewis MJ. Sharp leading edge hypersonic vehicles in the air and beyond. SAE Trans 1999;108(1):841–51.

[12] Paul Kolodziej, Moffett Field. Aerothermal performance constraints for hypervelocity small radius unswept leading edges and nosetips. NASA Technical Memorandum 112204; 1997.
[13] Chamberlain AL, Fahrenholtz W, Hilmas G, Ellerby D. Oxidation of ZrB_2-SiC ceramics under atmospheric and reentry conditions. Refract Appl Tran 2005;1(2):1–8.
[14] Monteverde F, Bellosi A. Microstructure and properties of an HfB_2–SiC composite for ultra high temperature applications. Adv Eng Mater 2004;6(5):331–6.
[15] Gasch M, Ellerby D, Irby E, Beckman S, Gusman M, Johnson S. Processing, properties and arc jet oxidation of hafnium diboride/silicon carbide ultra high temperature ceramic. J Mater Sci 2004;39(19):5925–37.
[16] Han JC, Hu P, Zhang XH, Meng SH, Han WB. Oxidation resistant ZrB_2 –SiC Composites at 2200 C. Compos Sci Technol 2008;68(3–4):799–806.
[17] Zhu Sumin, Fahrenholtz William G, Hilmas GE. Influence of silicon carbide particle size on the microstructure and mechanical properties of zirconium diboride–silicon carbide ceramics. J Eur Ceram Soc 2007;27:2077–83.
[18] Monteverde F, Bellosi A. Oxidation of ZrB_2-based ceramics in dry air. J Electrochem Soc 2003;150(11):B552–9.
[19] Rezaie Alireza, Fahrenholtz WG, Hilmas GE. Evolution of structure during the oxidation of zirconium diboride–silicon carbide in air up to 1500 °C. J Eur Ceram Soc 2007;27:2495–501.
[20] Fahrenholtz WG. Thermodynamic analysis of ZrB_2–SiC oxidation: formation of a SiC-depletion region. J Am Ceram Soc 2007;90(1):143–8.